Nonlinear Dyn
https://doi.org/10.1007/s11071-023-08708-z

ORIGINAL PAPER

Bipedal walking control by using acceleration factor

Linqi Ye · Xueqian Wang · Houde Liu · Bin Liang · Bo Yuan

Received: 6 March 2022 / Accepted: 26 June 2023

Abstract Humans can walk efficiently in a certain speed range, while state-of-the-art biped robots can hardly walk as fast as humans. In this paper, we investigate how to walk faster for two simple 2D walking models (Zaytsev in IEEE Trans Robot 34:336–352, 2018), including an inverted pendulum (IP) model and a linear inverted pendulum (LIP) model. Firstly, open-loop analysis is conducted based on the two models. The concept of "acceleration factor" is proposed, which is a key parameter that affects the mid-stance velocity transition between steps. We find that the acceleration factor has a fixed correlation with the velocity transition trend, which is independent of the step length. The step length only affects the feasible range of the acceleration factor, which suggests that we can decouple the control of walking speed from step length. Based on this, we design walking controllers for both models, where the walking velocity and step length are controlled separately. With the proposed controller, closed-loop simulations are performed in the V-REP software, which achieves a mid-stance velocity of 2 and 6 m/s for IP walking and LIP walking, respectively. Besides, walking with varied step lengths along with speed regulation is also demonstrated. This work might be helpful to improve the walking speed of biped robots in the future.

Keywords Walking control · Bipedal walking · Bipedal robots · Legged locomotion

1 Introduction

Humans can walk very efficiently with two legs. At most time, human walking can be expressed as an inverted pendulum (IP), where the supporting leg is kept relatively straight and the body moves along an arc. Behind that, it has been proved that this IP walking gait is more energy-efficient compared to other gaits [2]. To imitate human walking, passive walking machines were created [3], which can walk down a gentle slope by gravity in a very humanlike way. Later, researchers added actuators to the machine which

L. Ye
Institute of Artificial Intelligence, Collaborative Innovation Center for the Marine Artificial Intelligence, Shanghai University, Shanghai, China
e-mail: yelinqi@shu.edu.cn

X. Wang (✉) · H. Liu (✉) · B. Yuan
Center of Intelligent Control and Telescience, Tsinghua Shenzhen International Graduate School, Tsinghua University, Shenzhen, China
e-mail: wang.xq@sz.tsinghua.edu.cn

H. Liu
e-mail: liu.hd@sz.tsinghua.edu.cn

B. Liang
Navigation and Control Research Center, Department of Automation, Tsinghua University, Beijing, China

Published online: 09 July 2023

enables it to walk on level ground [4–6]. They are usually called as limit-cycle walkers, which are energy-efficient and only requires minimum control during walking.

Although IP walking is energy-efficient, it has an inherent limitation on the walking speed. Due to the circular motion of the body, the centrifugal force will pull the supporting leg to leave the ground when walking too fast. It can be calculated that the top speed of IP walking is about 3.16 m/s for a center of mass (CoM) height of 1 m [7]. Therefore, IP walking cannot be used anymore if we want to walk faster, for example, in race walking which aims at walking as fast as possible. Actually, the race-walking athletes walk in a quite unusual way with distinct hip twisting. Human studies [8] found that several mechanisms were used by the race walkers to minimize the vertical excursion of the CoM during race walking, which results in a much more flat CoM vertical trajectory compared to normal walking as can be seen from Fig. 1. In this way, the race walker can walk with an average speed of 3.3 m/s and a peak speed up to 4.6 m/s [9]. Actually, it can be computed that the top walking speed is $\sqrt{gR}$, where g is the acceleration of gravity and R is the curvature radius of the CoM trajectory. Obviously, the top walking speed increases as R increases.

As an extreme case, when $R \to \infty$, the CoM will move along a horizontal line, which results in level walking. This can be seen when people walk gingerly to prevent sloshing when holding a cup of water. In this case we bend our leg to keep a constant body height. This walking gait can be modelled as a linear inverted pendulum (LIP), which has been intensively studied in ZMP-based walking [10]. Although we rarely use LIP walking since it is more tiring, it is widely used in humanoid robots such as Asimo and HRP-4C [10].

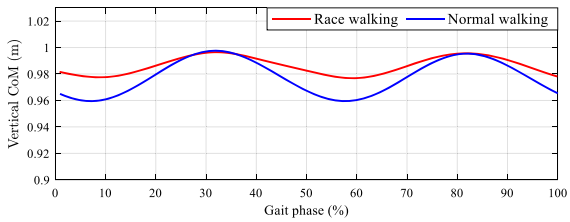

Fig. 1 Mean vertical CoM trajectory for race walking and normal walking. Data are reproduced from [8]

Technically speaking, LIP walking has no speed limitation provided we can swing our leg fast enough. However, as far as we know, the state-of-the-art biped robots can hardly walk as fast as human. For example, ASIMO's walking speed is set at 0.44 m/s, and a special experimental version has achieved 0.89 m/s [11]. COMAN [12] can walk at 0.9 m/s and MABEL [13] achieves 1.5 m/s walking. The recent work on ATRIAS has demonstrated high-speed walking of 2.2 m/s before it switches to running [14]. A more accurate comparison using dimensionless velocity can be found from Table 3 in [13], which also indicates a velocity gap that biped robots lag behind human. On one hand, this gap may come from the limited motor capability. This can be potentially solved by using high-torque density motors, such as brushless DC motors, which have been recently applied to quadruped robots and achieved a super-fast running speed [15]. On the other hand, walking faster is more difficult to control. In IP walking, the velocity is usually controlled by pushing off and modifying the step length [4–6]. While in LIP walking, the velocity is usually controlled by modifying the touch down timing [10]. However, there are some drawbacks in the existing methods. For example, the walking velocity and step length control are usually coupled.

In order to explore how to walk faster, we have taken human walking experiments. The results show that IP walking can hardly exceed 3 m/s, while LIP walking can easily achieve higher speed, for example, 4 m/s. To explain it, we do theoretical analysis for both IP and LIP walking using the concept of "acceleration factor" and some important features are discovered. Next, we design controllers for both IP and LIP walking using a separation principle, where the walking velocity is controlled through the acceleration factor and the step length can be adjusted freely to meet additional foot placement requirements. Finally, the effectiveness of the proposed method is demonstrated through simulations on a simple biped robot in V-REP [16].

The contributions of this paper are threefold. First, the question of "how to walk faster" is fully elaborated from both theoretical analysis and physical simulations by comparing IP and LIP walking. All results demonstrate that LIP walking can be faster than IP walking. This paper can help us better understand the strategy people take in race walking and improve the walking speed of biped robots in the future.

Second, the concept of acceleration factor is proposed, which gives a unified framework to study both IP and LIP walking. Third, we propose a new walking control method based on acceleration factor and demonstrate that walking speed and step length can be controlled separately with this method. This is particularly useful when doing fast walking on terrains with random gaps.

The remainder of this paper is organized as follows. Theoretical analysis of IP and LIP walking are conducted in Sects. 2 and 3, respectively. Walking controller is designed in Sect. 4 and the simulation results are given in Sect. 5. Finally, limitations and future work are presented in Sect. 6 and conclusions are given in Sect. 7.

2 Walking analysis

2.1 The IP walking model

The IP walking model is depicted in Fig. 2. The model has a point mass on the hip (the CoM) and two massless legs with point feet. The leg is telescopic to make ground clearance. During walking, the stance leg keeps a constant length and the CoM moves along an arc, while the swing leg is shortened to avoid scuff on the ground. When the swing leg touches the ground, it becomes the new stance leg and the previous stance leg starts to swing. The double stance phase is instantaneous.

The walking model is a hybrid system which consists of a continuous phase and a switch phase. During the continuous phase, the stance leg acts as an inverted pendulum which is governed by the equation as follows

$$\ddot{\theta} = g \sin\theta / L \tag{1}$$

where θ is the stance leg angle and L is the length of the leg.

During the switch phase, two impulsive forces from the ground are exerted to the robot along the two legs. One is the heel strike $\vec{H}$ acts on the leading leg and the other is the push off $\vec{P}$ applied to the trailing leg (push off is assumed to happen just before heel strike). The impulse forces result in a sudden change on the CoM velocity, which is governed by [7]

$$\dot{\theta}^+ = \dot{\theta}^- \cos(2\theta^-) + P \sin(2\theta^-)/(mL) \tag{2}$$

where P is the amplitude of the push off $\vec{P}$ and m is the mass, θ^-, θ^+ are the stance leg angles just before and after switch, respectively. After switch, the former stance leg becomes the new stance leg, so we have $\theta^+ = -\theta^-$.

Comment 1: Equation (2) can also be expressed by H since the magnitude of the impulse $\vec{P}, \vec{H}$ are coupled as can be seen from Fig. 2 ($m\overrightarrow{V^+} - m\overrightarrow{V^-} = \vec{P} + \vec{H}$, $\vec{P} \perp \overrightarrow{V^-}$, $\vec{H} \perp \overrightarrow{V^+}$).

For this model, the stance leg compression should always be nonnegative to maintain foot contact with the ground, which poses the following constraint.

IP walking constraint: stance leg nonnegative compression

$$mg\cos\theta - mL\dot{\theta}^2 \geq 0 \tag{3}$$

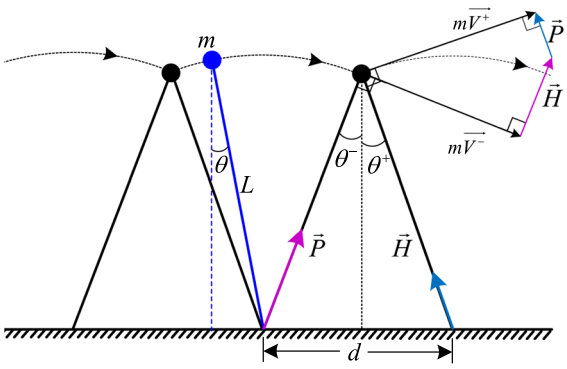

Fig. 2 The inverted pendulum (IP) walking model. (d is step length)

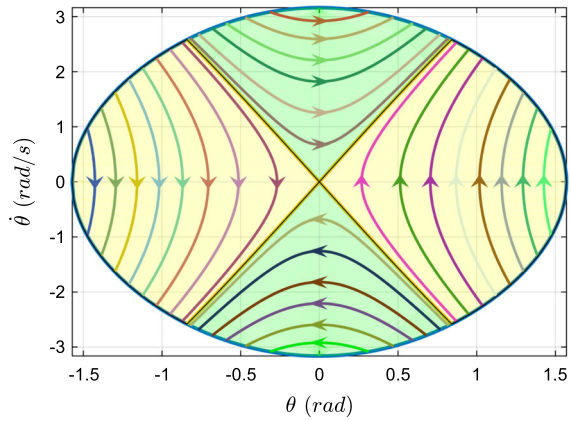

Fig. 3 The phase portrait of IP walking

It can be simplified as

$$\dot{\theta} \leq \sqrt{g \cos \theta / L} \tag{4}$$

With (1) and (4), we plot the phase portrait of IP walking in Fig. 3 (L set to 1 m and g uses 10 m/s^2).

It can be observed that the phase portrait is constrained in an oval area, with the highest mid-stance velocity of about 3.16 m/s, which is an inherent limitation on the walking speed of IP walking.

2.2 The acceleration factor for IP walking

From the phase portrait in Fig. 3, it can be seen that the walking velocity during a step follows a pre-determined curve which cannot be modified once the initial velocity is given. Therefore, we can use the mid-stance velocity (when $\theta = 0$) to represent the walking velocity in a step. To regulate the walking speed, we need to control the mid-stance velocity transition between steps. For IP walking, the velocity transition is influenced by the push off as can be seen from (2). Theoretically speaking, the amount of needed push off can be calculated from (2) for a desired velocity in the next step. However, the calculated push off is an impulse, which is impossible to perform in practice. Therefore, we need to consider another feasible method to control the velocity transition between steps. To this end, we propose the concept of acceleration factor.

An acceleration factor should have the following features: (1) An acceleration factor is a state variable that can be conveniently controlled during walking; (2) An acceleration factor has a direct correlation with the velocity transition between steps. Feature 1 requires that an acceleration factor can be measured and can be controlled by the available input. Feature 2 indicates that we know how the mid-stance velocity changes in the next step for a given value of the acceleration factor.

To find an appropriate acceleration factor, three cases of velocity transition are depicted in Fig. 4, which corresponds to deceleration, equal-velocity, and acceleration, respectively.

In Fig. 4, V_t is the CoM velocity just after push off. By examining the three cases, we find a key parameter which affects the velocity transition, that is, the angle of V_t, which is denoted by α in Fig. 4. Formally, we define the acceleration factor for IP walking as

$$a_{ip} = \tan \alpha = V_t^z / V_t^x \tag{5}$$

where V_t^z, V_t^x are the vertical and horizontal component of V_t, respectively.

This definition satisfies the two aforementioned requirements. First, a_{ip} is the ratio of the vertical component and the horizontal component of the CoM velocity, which can be measured through the joint encoders and can also be controlled through the joint actuators. Second, the correlation of a_{ip} with the velocity transition is clear. That is, $a_{ip} < 0$ indicates deceleration, $a_{ip} = 0$ indicates maintaining the same velocity, and $a_{ip} > 0$ indicates acceleration.

Since the ground forces $\vec{P}$ and $\vec{H}$ always point upwards, α is limited by $-\theta_t \leq \alpha \leq \theta_t$. Therefore, the acceleration factor is constrained by

$$-\tan \theta_t \leq a_{ip} \leq \tan \theta_t \tag{6}$$

where $\theta_t > 0$ is the leg angle at transition, which is related to the step length by

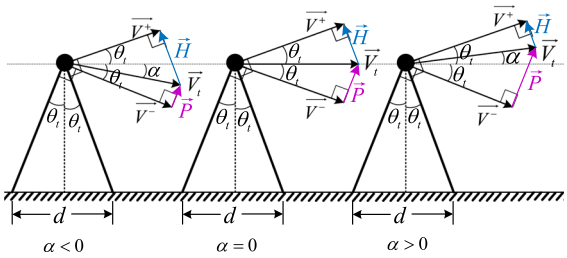

Fig. 4 Velocity transition in IP walking. **a** $\alpha < 0$ results in deceleration; **b** $\alpha = 0$ maintains the same velocity; **c** $\alpha > 0$ results in acceleration

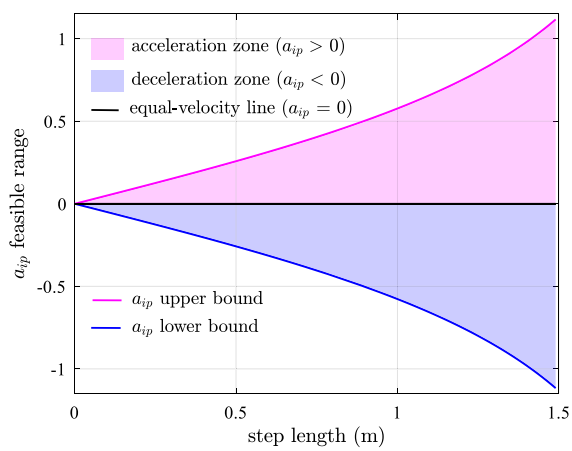

Fig. 5 The feasible range of a_{ip} for different step lengths

$$\theta_t = \text{asin}[d/(2L)] \tag{7}$$

Substituting (7) into (6), the relationship between the acceleration factor and the step length is

$$-d/\sqrt{4L^2 - d^2} \le a_{ip} \le d/\sqrt{4L^2 - d^2} \tag{8}$$

Using (8), the feasible range of a_{ip} with respect to different step lengths is drawn in Fig. 5. It can be observed that the feasible range of a_{ip} increases with the step length, which forms a trumpet shape. The upper bound and lower bound are symmetric about the equal-velocity line.

For a given value of a_{ip}, the relationship of the mid-stance velocity between two successive steps can be calculated. Denote the mid-stance velocity of two successive steps as V_k and V_{k+1}, respectively. During a step, the kinetic energy is conserved, so we have

$$V_k^2 + 2gL = (V^-)^2 + 2gL\cos\theta_t \tag{9}$$

$$V_{k+1}^2 + 2gL = (V^+)^2 + 2gL\cos\theta_t \tag{10}$$

where V^-, V^+ are the CoM velocity just before and after switch, respectively.

From (9), (10) we can solve that

$$V^- = \sqrt{V_k^2 + 2gL(1 - \cos\theta_t)} \tag{11}$$

$$V_{k+1} = \sqrt{(V^+)^2 - 2gL(1 - \cos\theta_t)} \tag{12}$$

Moreover, from Fig. 4, we have

$$V_t = V^-/\cos(\theta_t + \alpha) \tag{13}$$

$$V^+ = V_t\cos(\theta_t - \alpha) = V^-\cos(\theta_t - \alpha)/\cos(\theta_t + \alpha) \tag{14}$$

Substituting (14) and (11) into (12) yields

$$V_{k+1} = \sqrt{\left[V_k^2 + 2gL(1 - \cos\theta_t)\right]\frac{\cos^2(\theta_t - \alpha)}{\cos^2(\theta_t + \alpha)} - 2gL(1 - \cos\theta_t)} \tag{15}$$

Equation (15) describes the mid-stance velocity transition between two successive steps. With (15), the mid-stance velocity transition curve for IP walking is plotted in Fig. 6. The black line represents the equal-velocity line, which corresponds to $a_{ip} = 0$. Above the black line is the acceleration zone, while under it is the deceleration zone.

From Fig. 6 we can get some useful information: (1) The acceleration factor a_{ip} has an invariable relationship with the velocity transition trend which is independent of the step length. Indeed,$a_{ip} = 0$, $a_{ip} < 0$, and $a_{ip} > 0$ always indicate equal-velocity, deceleration, and acceleration, respectively, no matter what the step length is; (2) The step length has an influence on the velocity transition range, that is, a bigger step leads to a wider velocity range for the next step; (3) The velocity transition curves for $a_{ip} = \pm a$ (and for the same d) are symmetric (strictly symmetric which can be proved theoretically from (15)) about the equal-velocity line.

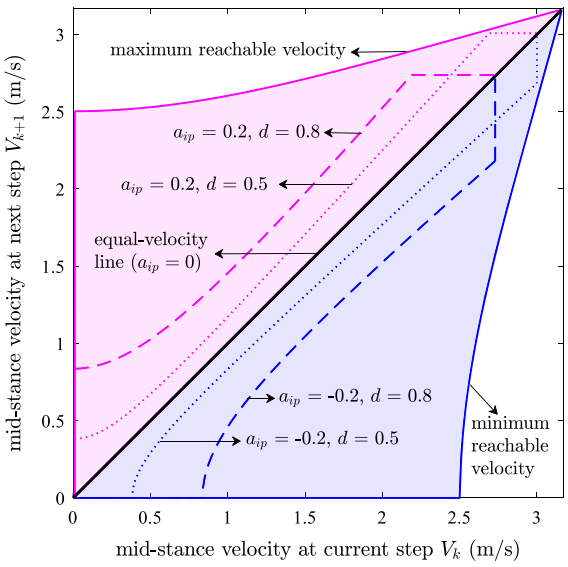

Fig. 6 Velocity transition curve for IP walking

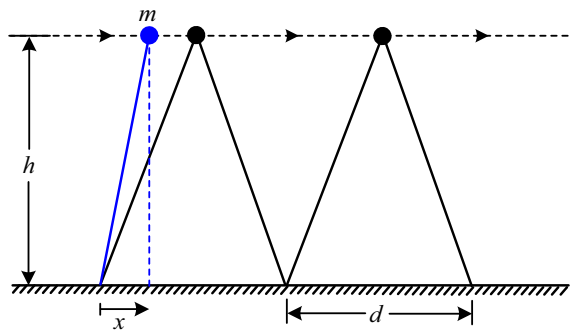

Fig. 7 The linear inverted pendulum (LIP) walking model

3 Lip walking analysis

3.1 The LIP walking model

The LIP walking model is depicted in Fig. 7. This model also has a point mass on the hip and two massless legs with point feet. The difference with IP walking is that the stance leg changes its length during LIP walking to maintain a constant CoM height ($h = 1\,\text{m}$ is used in this paper). And the leg transition happens in a smooth way where the CoM velocity maintains the same, in contrast to the abrupt velocity change in IP walking. The double stance phase is also assumed to be instantaneous.

During the continuous phase, the system follows the dynamics of a linear inverted pendulum, which is

$$\ddot{x} = gx/h \tag{16}$$

where x is the horizontal position of the hip relative to the stance foot.

In leg transition, the former swing leg becomes the new stance leg, so we have

$$x^+ = x^- - d,\ \dot{x}^+ = \dot{x}^- \tag{17}$$

where d is the step length.

In LIP walking, the leg length has a maximum value, which puts the following constraint on x.

LIP walking constraint: leg length constraint

$$x^2 + h^2 \le l_{\max}^2 \tag{18}$$

where $l_{\max} > 0$ is the maximum leg length.

With (16) and (18), the phase portrait of LIP walking is presented in Fig. 8.

In Fig. 8, the left and right boundaries are caused by the leg length constraint ($l_{\max} = 1.2$ is used). The upper and lower boundaries are determined by the leg swing speed. If the leg can swing as fast as we want, then there is no limitation on the walking speed.

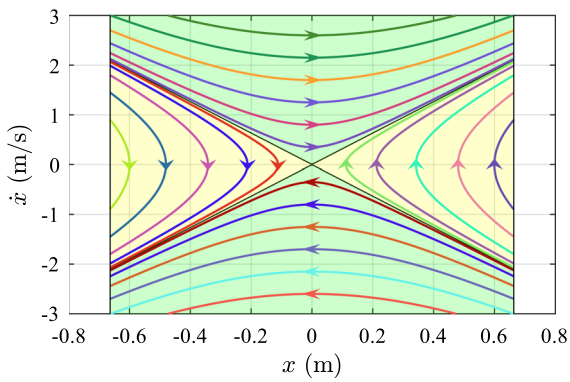

Fig. 8 The phase portrait of LIP walking

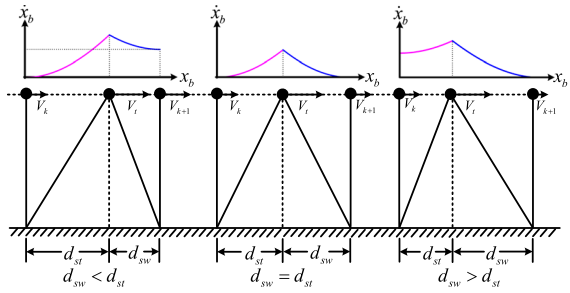

Fig. 9 Velocity transition in LIP walking. x_b represents the absolute horizontal position of the body

3.2 The acceleration factor for LIP walking

Unlike IP walking, the CoM velocity keeps unchanged during leg transition in LIP walking. However, the mid-stance velocity changes if the swing leg and stance leg are asymmetric during leg transition, which is very similar to that observed in running [17]. Figure 9 shows three cases of velocity transition for LIP walking, where d_{st} is the distance from the stance foot to the CoM and d_{sw} is the distance from the swing foot to the CoM. As can be seen from the top part, the CoM velocity increases before leg transition and decreases after leg transition. If $d_{sw} < d_{st}$, it accelerates more so that the mid-stance velocity will increase; if $d_{sw} = d_{st}$, the velocity curve is symmetric and the mid-stance velocity remain unchanged; if $d_{sw} > d_{st}$, it decelerates more so that the mid-stance velocity will decrease.

Formally, we define the acceleration factor for LIP walking as

$$a_{lip} = d_{sw}/d_{st} \tag{19}$$

This definition also satisfies the two aforementioned requirements. First, a_{lip} can be measured through joint encoders and can be controlled through the hip actuator of the swing leg. Second, the correlation of a_{lip} with velocity transition is clear. That is, $a_{lip} > 1$ indicates deceleration, $a_{lip} = 1$ indicates maintaining the same velocity, and $a_{lip} < 1$ indicates acceleration.

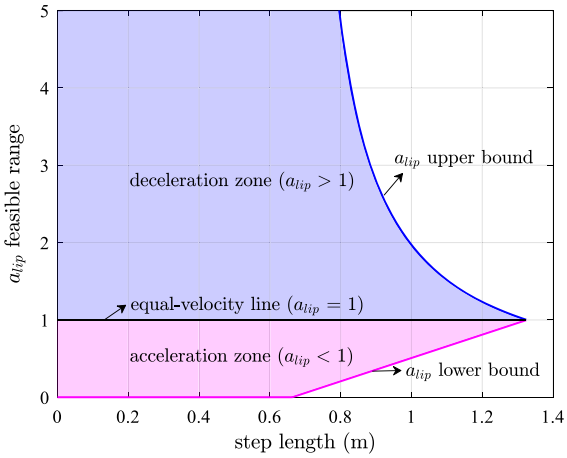

Fig. 10 The feasible range of a_{lip} for different step lengths

We assume that the CoM always locates between the stance foot and swing foot during leg transition. Therefore, the boundary of a_{lip} is

$$\begin{cases} 0 \le a_{lip} \le +\infty, & \text{if } d \le d_m \\ \dfrac{d-d_m}{d_m} \le a_{lip} \le \dfrac{d_m}{d-d_m}, & \text{if } d > d_m \end{cases} \tag{20}$$

where $d_m = \sqrt{l_{\max}^2 - 1}$ is the upper limit for d_{st} and d_{sw}.

With (20), the feasible range of a_{lip} with respect to different step lengths is drawn in Fig. 10. It can be observed that the feasible range of a_{lip} decreases with the step length when $d > d_m$.

Similar to the IP case, the relationship of the mid-stance velocity between two successive steps can be derived. During a step, the "orbital energy" [10] $E = \dot{x}^2/2 - gx^2/2h$ is conserved, so we have

$$\begin{aligned} hV_k^2 &= hV_t^2 - gd_{st}^2 \\ hV_{k+1}^2 &= hV_t^2 - gd_{sw}^2 \end{aligned} \tag{21}$$

From above we can solve that

$$V_{k+1} = \sqrt{V_k^2 + g(d_{st}^2 - d_{sw}^2)/h} \tag{22}$$

Moreover, since $d = d_{st} + d_{sw}$ and $d_{sw} = a_{lip} d_{st}$, it can be solved that

$$\begin{aligned} d_{sw} &= da_{lip}/(a_{lip}+1) \\ d_{st} &= d/(a_{lip}+1) \end{aligned} \tag{23}$$

Substituting (23) into (22) results in

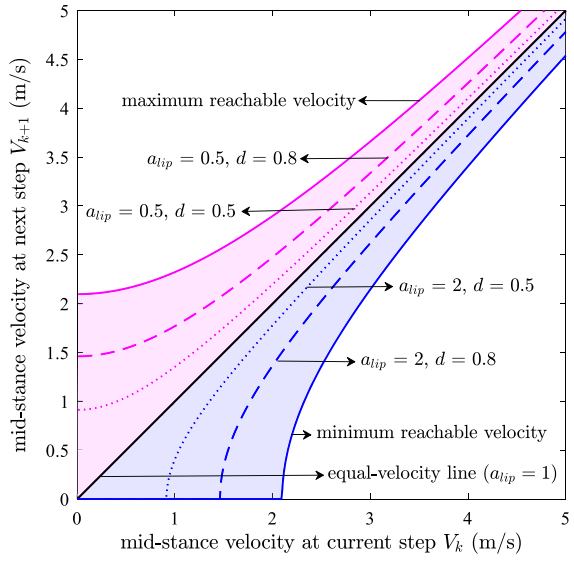

Fig. 11 Velocity transition curve for LIP walking

$$V_{k+1} = \sqrt{V_k^2 + gd^2(1 - a_{lip}^2)/h(a_{lip}+1)^2} \tag{24}$$

Using (24), the mid-stance velocity transition curve between two steps is plotted in Fig. 11.

From Fig. 11 we can get the following conclusions: (1) The acceleration factor a_{lip} has an invariable relationship with the velocity transition trend, which does not depend on the step length. Indeed,$a_{lip} = 1$, $a_{lip} > 1$, and $a_{lip} < 1$ always indicate maintaining speed, deceleration, and acceleration, respectively, no matter what the step length is; (2) The step length has an influence on the velocity transition range, that is, bigger step leads to a wider velocity range for the next step; (3) The velocity transition curves for $a_{lip} = a$ and $a_{lip} = 1/a$ are symmetric (strictly symmetric which can be proved theoretically from (24)) about the equal-velocity line.

Table 1 Acceleration factors in bipedal walking

	IP walking	LIP walking
Definition	$a_{ip} = V_t^z/V_t^x$	$a_{lip} = d_{sw}/d_{st}$
Feature	$a_{ip} = 0$: Equal-velocity	$a_{lip} = 1$: Equal-velocity
	$a_{ip} > 0$: Acceleration	$a_{lip} < 1$: Acceleration
	$a_{ip} < 0$: Deceleration	$a_{lip} > 1$: Deceleration

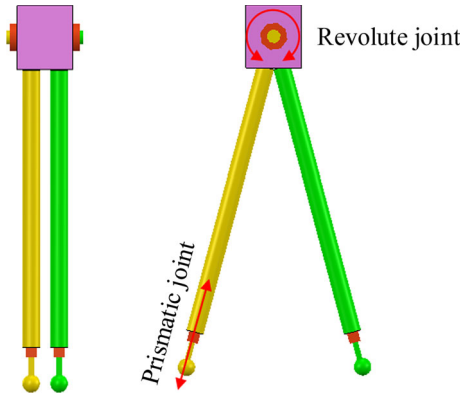

Fig. 12 Simulation model in V-REP

4 Walking controller design

With the open-loop analysis results obtained in the previous sections (summarized in Table 1), we are ready to design walking controllers for both IP and LIP walking.

To control the walking speed, we can simply use a bang-bang control law. For example, IP walking can use

$$a_{ip} = a_0 \text{sign}(V_r - V_k) \tag{25}$$

where $a_0 > 0$, and V_k, V_r are the measured and desired mid-stance velocity, respectively. However, in this way the walking speed will finally oscillate around the desired speed. As an improvement, we replace the sign function with a smooth saturation function:

$$a_{ip} = a_1 \tanh[\lambda_1(V_r - V_k)] \tag{26}$$

where $a_1, \lambda_1 > 0$ are parameters to be designed.

The interpretation of (26) is: when $V_k < V_r$, we have $a_{ip} > 0$ so the robot will accelerate; and when $V_k > V_r$, we have $a_{ip} < 0$ so the robot will decelerate. Therefore, the mid-stance velocity will approach the desired velocity V_r gradually.

And for LIP walking, the controller is designed as

$$a_{lip} = 1 + a_2 \tanh[\lambda_2(V_k - V_r)] \tag{27}$$

where $\lambda_2 > 0$ and $0 < a_2 < 1$ are parameters to be designed.

The interpretation of (27) is: when $V_k < V_r$, we have $a_{lip} < 1$ so the robot will accelerate; and when $V_k > V_r$, we have $a_{lip} > 1$ so the robot will decelerate. Therefore, the mid-stance velocity goes towards the desired velocity V_r gradually.

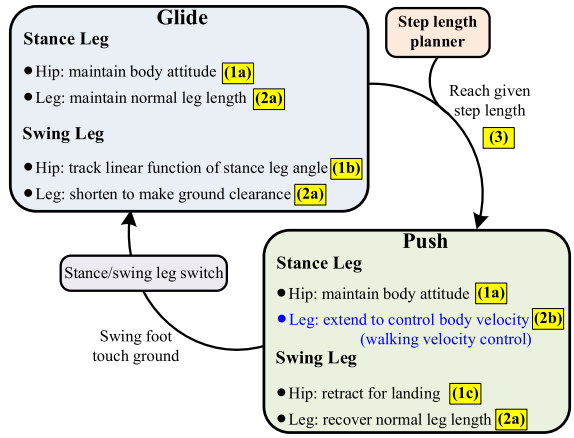

Fig. 13 IP walking control architecture

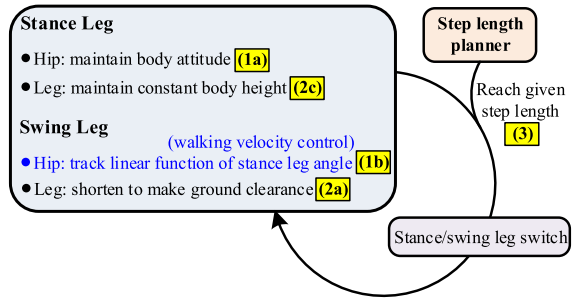

Fig. 14 LIP walking control architecture

To design full controllers, we consider a more practical walking model built in V-REP as shown in Fig. 12. The model has a cuboid body, two telescopic legs ended with small spherical feet. This model has four actuators in all, including two revolute joints connecting the body with each leg and two prismatic joints connecting each leg with the foot. The walker is constrained in 2D by two frictionless walls.

The overall control architecture for IP and LIP walking are given in Figs. 13 and 14, respectively. On the top level, a state machine is applied to manage the switch between the stance leg and the swing leg.

The low-level controllers include:

Hip controller (for the revolute joint on the hip)

(1a) Body attitude controller

The body is kept vertical by controlling the hip actuator of the stance leg with the torque:

$$\tau_{st} = -\tau_{sw} - k_p^b \theta_b - k_d^b \dot{\theta}_b \tag{28}$$

where θ_b is the pitch angle of the body and τ_{sw} is the torque from the hip joint of the swing leg. $k_p^b, k_d^b > 0$ are the proportional and derivative gains, respectively.

(1b) Swing leg controller

The swing leg is controlled by the hip actuator of the swing leg with the torque:

$$\tau_{sw} = -k_p^s(\theta_{sw} - \theta_r) - k_d^s \dot{\theta}_{sw} \tag{29}$$

where θ_{sw} is the swing leg angle and θ_r is the desired angle. $k_p^s, k_d^s > 0$ are the proportional and derivative gains, respectively.

Specifically, θ_r for IP walking is designed as

$$\theta_r = \begin{cases} -\theta_{st}, & \text{if } \theta_{st} \le 0 \\ -k_s \theta_{st}, & \text{if } \theta_{st} > 0 \end{cases} \tag{30}$$

where θ_{st} is the stance leg angle and $k_s > 1$ is a parameter. θ_r for LIP walking is designed as

$$\theta_r = \begin{cases} k_t \theta_{st}, & \text{if } \theta_{st} \le 0 \\ -\text{atan}\left(a_{lip} \tan \theta_{st}\right), & \text{if } \theta_{st} > 0 \end{cases} \tag{31}$$

where θ_{st} is the stance leg angle and k_t is the ratio of θ_{st}/θ_{sw} during the previous leg transition.

(1c) Leg retraction controller

A leg retraction controller is used for IP walking to let the swing leg rotate backward just before touching ground, which can enhance the walking stability [18]. We control the hip actuator of the swing leg with the torque

$$\tau_{sw} = -k_p^r(\dot{\theta}_{sw} - \omega_r) \tag{32}$$

where ω_r is the desired backward-swing speed, $k_p^r > 0$ is the proportional gain. In this paper $\omega_r = 4$ rad/s is adopted.

Leg controller (for the prismatic joint on the leg)

(2a) Leg length controller

The swing/stance leg length is controlled using velocity control mode for the prismatic joint

$$v_l = -k_p^l(l - l_r) \tag{33}$$

where $k_p^l > 0$ is the proportional gain, l, l_r are the measured and desired leg lengths, respectively. In this paper, $l_r = 1$ m is used for the stance leg in IP walking and $l_r = 0.98$ m is used for the swing leg to make ground clearance.

(2b) Body velocity controller

Comment 2: "Body" refers to the link that connects both legs, and the body of our simulation model is the pink cube shown in Fig. 12. As the cube has most of the robot's mass, it's considered as the center of mass to design the controller. Accordingly, "body velocity" refers to the cube velocity relative to the world frame, which is an approximation of the "CoM velocity" of the point-mass model as mentioned in the previous sections.

In IP walking, the body velocity during leg transition is controlled by setting the force on the prismatic joint of the stance leg as:

$$F_{st} = \left[m_b g - k_p^v\left(V_b^z - a_{ip} V_b^x\right)\right] / \cos\theta_{st} \tag{34}$$

where $k_p^v > 0$ is the proportional gain, m_b is the body mass, V_b^z and V_b^x are the body velocity in the vertical and horizontal axes, respectively.

(2c) Body height controller

In LIP walking, the body height is maintained constant by controlling the prismatic joint of the stance leg with the force:

$$F_{st} = \left[m_b g - k_p^h(z_b - h_r) - k_d^h \dot{z}_b\right] / \cos\theta_{st} \tag{35}$$

where $k_p^h, k_d^h > 0$ are the proportional and derivative gains, respectively. z_b, h_r are the measured and desired body heights, respectively. In this paper $h_r = 1$ m is adopted.

Leg transition trigger

The leg transition trigger is used to control the step length by checking if $d_e \ge d_r$, where d_e, d_r are the estimated and desired step lengths, respectively.

In IP walking, the estimated step length is

$$d_e = 2L \sin\theta_{st} \tag{36}$$

where L is the constant leg length (1 m in this paper).

In LIP walking, the estimated step length is

$$d_e = (1 + a_{lip}) h \tan\theta_{st} \tag{37}$$

where h is the constant body height (1 m in this paper).

With the above controllers, walking velocity and step length can be controlled separately for both IP and LIP walking. Here we call it as the separation principle.

5 Simulation results

To test the effectiveness of the proposed walking controller, simulations are performed in V-REP [16] with the model shown in Fig. 12. Newton physics engine is adopted and the time step is 0.01 s. The mass of the body, the leg, and the foot are 10, 0.6, and 0.2 kg, respectively. The moment of inertia for each part is computed automatically by V-REP. The maximum torque for the revolute joint is 100 Nm and the maximum force for the prismatic joint is 300 N. We offer three video attachments for the simulation which are highly recommended to watch. The controller parameters are listed in Table 2.

Comment 3: A fine tuning of the parameters can possibly lead to faster walking speed. However, walking too fast is not easy even for human—we tend to transit to running when we need to go faster.

5.1 Walking with fixed step length

Firstly, we simulate walking with a fixed step length $d_r = 0.6$ m to find out how fast our controller can achieve for the two walking gaits.

For IP walking, a mid-stance velocity of 2 m/s is achieved when setting $V_r = 2$ m/s. While for LIP walking, a mid-stance velocity of 6 m/s is achieved when setting $V_r = 6.2$ m/s. The results are shown in Figs. 15 and 16, which show the walking velocity with respect to the body horizontal position.

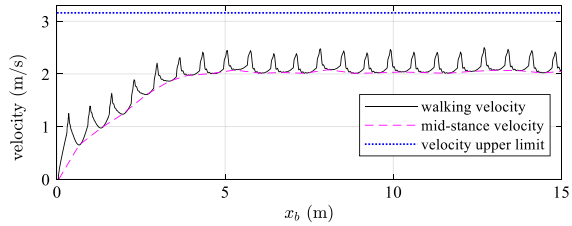

Fig. 15 Simulation results of IP walking with fixed step length

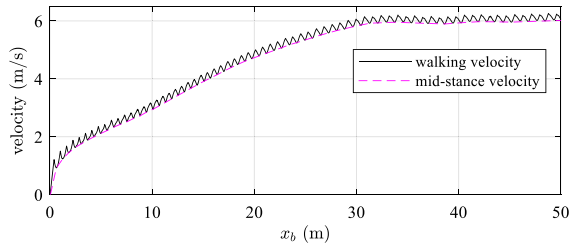

Fig. 16 Simulation results of LIP walking with fixed step length

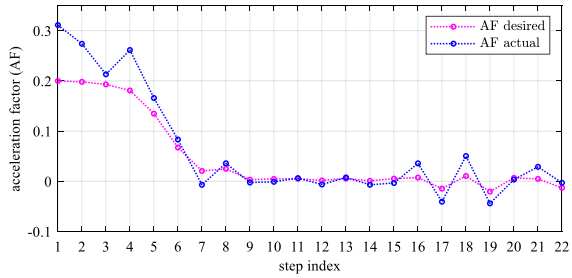

Fig. 17 The acceleration factor value during IP walking

Moreover, to analyze the control accuracy of the acceleration factor, we take IP walking as an example and show the actual and desired values of the

Table 2 Controller parameters

	IP walking		LIP walking	
Hip controller	(1a)	$k_p^b = 500$, $k_d^b = 10$	(1a)	$k_p^b = 500$, $k_d^b = 10$
	(1b)	$k_p^s = 300$, $k_d^s = 10$,$k_s = 1.4$	(1b)	$k_p^s = 300$,$k_d^s = 10$,$a_2 = 0.25$,$\lambda_2 = 4$
	(1c)	$k_p^r = 10$		
Leg controller	(2a)	$k_p^l = 30$(swing leg), $k_p^l = 5$(stance leg)	(2a)	$k_p^l = 30$,
	(2b)	$k_p^v = 500$,	(2c)	$k_p^h = 1000$, $k_d^h = 500$
		$a_1 = 0.2$,$\lambda_1 = 2$		

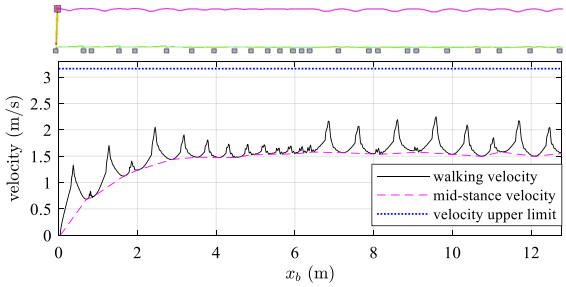

Fig. 18 Simulation results of IP walking with varied step length

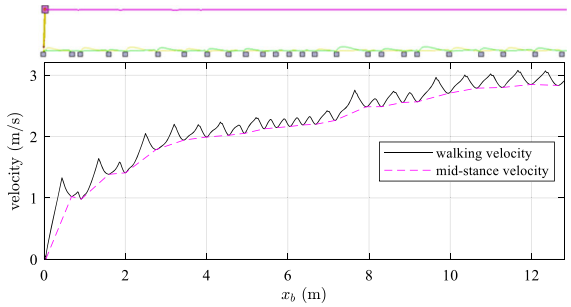

Fig. 19 Simulation results of LIP walking with varied step length

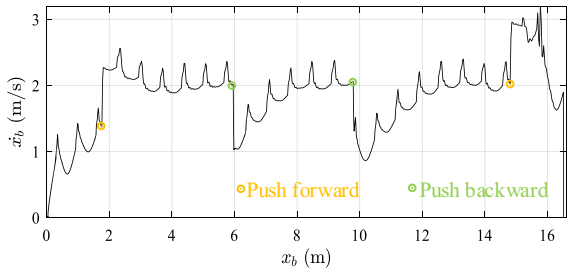

Fig. 20 Simulation results of IP walking with disturbance

acceleration factor in Fig. 17 (same simulation setting as in Fig. 15).

From Fig. 17, It can be seen that the general trends of the two curves are highly consistent. However, the acceleration factor is not accurately controlled (and not needed), which can be explained as follows. Firstly, the intermittent property of acceleration factor prevents it to be exactly controlled. In our definition, acceleration factor is a variable related to velocity transition between steps, which is defined in the step switch instant (foot touch down). Therefore, the precise value of the acceleration factor cannot be known until the step switch happens, which means a lack of feedback information to control it directly. Indeed, the acceleration factor is controlled indirectly (through the swing angle, step timing, etc.), which causes a control error inevitably (the control error cannot be obtained before step switch, and when step switch happens (instantaneously), there is no more chance to adjust). Second, the acceleration factor does not need to be exactly controlled, since the acceleration factor is not our final control goal, but the walking velocity is. So, it is ok if the acceleration factor deviates from the desired value but can lead to the same velocity transition trend. As can be seen from Fig. 17, the actual AF mostly locates on the same side of the zero line (which is the dividing line of acceleration/deceleration for IP walking) with the desired AF (despites some points very close to zero). This explains why the AF is not exactly controlled, but the desired walking velocity can still be achieved.

5.2 Walking with varied step length

Then we simulate walking with varied step length by letting the robot walk on a row of randomly distributed blocks (each block has a width of 0.12 m).

The distance between two adjacent blocks ranges from 0.2 to 0.8 m. During simulation, the step length planner obtains the distance between the next block and its stance foot in real time and set it as the desired step length. The desired velocity is set to $V_r = 1.5$ m/s for IP walking and $V_r = 3$ m/s for LIP walking. The simulation results are shown in Figs. 18 and 19.

It can be seen from the video that the robot successfully steps on all the blocks in both situations. Particularly, for IP walking, the robot achieves 1.5 m/s mid-stance velocity after walking for a distance of 4 m. While for LIP walking, the robot keeps accelerating and reaches a mid-stance velocity a little smaller than 3 m/s. Moreover, it can be observed from both figures that the robot accelerates more when taking a longer step before reaching the desired velocity, which is consistent with the conclusion obtained from the open-loop analysis. Finally, the control objective for both walking velocity and step length are achieved, which verifies the effectiveness of the proposed separation control strategy.

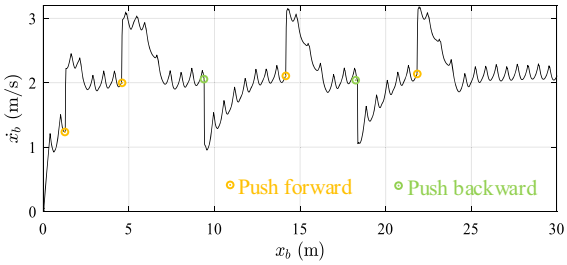

Fig. 21 Simulation results of LIP walking with disturbance

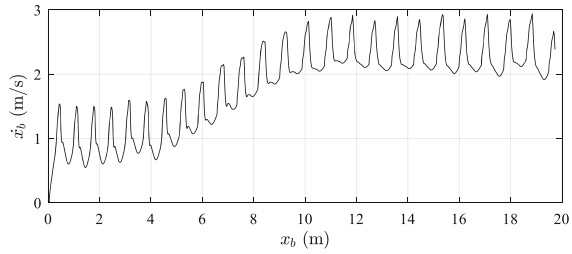

Fig. 22 Simulation results of IP walking with heavy legs

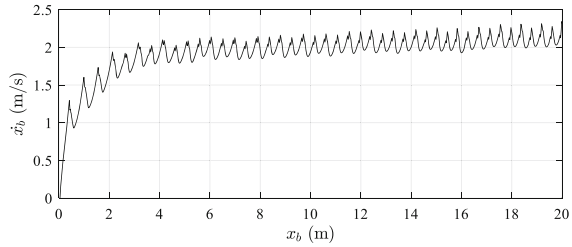

Fig. 23 Simulation results of LIP walking with heavy legs

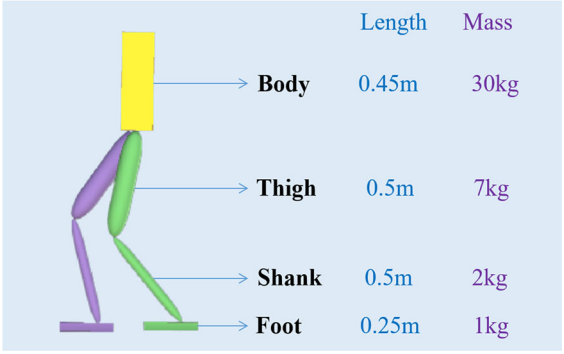

Fig. 24 A full biped model used for simulation

5.3 Robustness test

To test the robustness of the proposed controller, two scenarios are considered here.

The first is external disturbance. The robot is commanded to walk at 2 m/s and an impulsive external force is added to the robot intermittently during simulation. The force is 1000 N (forward or backward) added to the body center and lasts for 0.01 s, which results in an abrupt velocity change of about 1 m/s to the robot. The simulation results of IP and LIP walking are shown in Figs. 20 and 21, respectively.

For IP walking, it can be seen from Fig. 20 that the robot can recover to the target velocity if the perturbed velocity is not too high. But when the perturbed velocity goes to about 3 m/s, then the stance leg leaves the ground and the robot falls (see the attached video). While for LIP walking, the robot is more robust to external disturbance. As can be seen from Fig. 21, even when the perturbed velocity goes beyond 3 m/s, the robot can still recover to the target velocity. However, this does not necessarily mean that IP walking is less robust than LIP walking. Actually, people can take other measures to avoid falling during IP walking, for example, transit to running when the velocity is high. We may also use a switch control strategy to enhance the robustness of the IP walking controller.

The second consideration is model uncertainty. In the previous simulation, the leg mass of the robot is much smaller compared to the body mass (body 10 kg, leg with foot 0.8 kg). However, for a real humanoid robot, the leg might be very heavy. To test if the controller still works in this case, we increase the leg mass to half of the body mass (body 10 kg, each leg with foot 5 kg). The simulation results for IP and LIP walking are shown in Figs. 22 and 23, respectively. It can be observed that the robot can still achieve the commanded velocity (2 m/s), although may need to take more steps as can be found by comparing Figs. 15 and Fig. 22. This indicates that the proposed controller has some adaptability to biped robots with heavy legs, although the controller is derived from idealized model with massless legs.

5.4 Full biped simulation

To further test the effectiveness of the controller, we build a full biped simulation model as shown in Fig. 24.

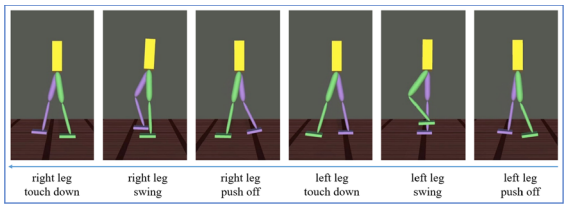

Fig. 25 IP walking snapshots in a gait cycle for the full biped model

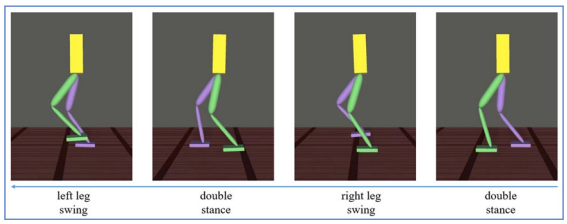

Fig. 26 LIP walking snapshots in a gait cycle for the full biped model

This model has similar parameters to a real biped robot that is undergoing in our lab. By using the acceleration factor method, we successfully achieve fast and stable walking for the full biped model (see Figs. 25 and 26, and the attached video). Specifically, 1.8 m/s is achieved for IP walking and 3 m/s is achieved for LIP walking in the simulation, which further verifies the effectiveness of the acceleration factor method.

6 Limitations and future work

This analysis in this paper is based on an idealized model with a point mass on the hip and legs without mass. In the real world, due to the complexity of mechanical structure, the robot's CoM is difficult to calculate and the dynamics are coupled with the movement of the legs so it's hard to place the foot accurately. The errors caused by these problems can be reduced by designing specific compensation or feedforward controllers. It is also hard to model a motor precisely and the control errors become significant when walking quickly. Recently researchers have tried using deep learning to build accurate motor models and achieved good results.

We are now building a real biped robot whose leg has a significant mass (1/3 of the body mass for single leg), making it quite different from the point-mass model. Heavy limbs bring a challenge for our controller design as the relationship between the acceleration factor and velocity transition may change and the conclusions obtained from the point-mass model has less fidelity. We are going to validate our theory about the acceleration factor on the real robot and solve this problem in future research.

7 Conclusion

Biped walking research usually focus on robustness, stability, and efficiency, while how to walk fast seems to be rarely studied. This paper attempts to answer this question. We study two kinds of biped walking gaits, namely IP walking and LIP walking, and propose a new strategy to control the walking velocity by using acceleration factor. We demonstrate that LIP walking can be faster than IP walking from both theoretical analysis and physical simulations. Particularly, we achieve a mid-stance velocity of 6 m/s for LIP walking in simulation. Besides, the proposed strategy removes the coupling on the control of walking velocity and step length, making it possible to adjust step length while regulating speed. This is particularly useful when doing fast walking on terrains with random gaps, which is even a challenging task for human. Although this paper uses simplified models, the results may facilitate controller design for more sophisticated real biped robots.

Funding This work was supported by the National Natural Science Foundation of China under Grant No. 62003188 and Grant No. 92248304, The Shenzhen Science Fund for Distinguished Young Scholars (RCJC20210706091946001).

Data availability The authors declare that the data supporting the findings of this study are available within the article and the video attachment.

Declarations

Conflict of interest The authors declare that they have no conflict of interest.

References

1. Zaytsev, P., Wolfslag, W., Ruina, A.: The boundaries of walking stability: Viability and controllability of simple models. IEEE Trans. Robot. **34**(2), 336–352 (2018)

2. Srinivasan, M., Ruina, A.: Computer optimization of a minimal biped model discovers walking and running. Nature **439**(7072), 72–75 (2006)
3. McGeer, T.: Passive dynamic walking. Int. J. Robot. Res. **9**, 62–82 (1990)
4. Collins, S., Ruina, A., Tedrake, R., Wisse, M.: Efficient bipedal robots based on passive-dynamic walkers. Science **307**, 1082–1085 (2005)
5. Bhounsule, P.A., Cortell, J., Grewal, A., Hendriksen, B., Karssen, J.D., Paul, C., Ruina, A.: Low-bandwidth reflex-based control for lower power walking: 65 km on a single battery charge. Int. J. Robot. Res **33**, 1305–1321 (2014)
6. Hobbelen, D.G., Wisse, M.: Controlling the walking speed in limit cycle walking. Int. J. Robot. Res. **27**(9), 989–1005 (2008)
7. Ye L. and Chen X..: Understand human walking through a 2D inverted pendulum model. in *IEEE-RAS International Conference on Humanoid Robots (Humanoids)*, pp. 340–345, 2018.
8. Norberg, J.D.: Biomechanical analysis of race walking compared to normal walking and running gait. University of Kentucky, Lexington, Kentucky (2015)
9. Lau C.: Speed of the fastest human walking. in *The physics factbook: An encyclopedia of scientific essays*, online.
10. Kajita, S., Hirukawa, H., Harada, K., Yokoi, K.: Introduction to humanoid robotics. Springer, Heidelberg, Berlin (2014)
11. "Asimo Frequently Asked Questions," online, available at https://asimo.honda.com/downloads/pdf/honda-asimo-robot-fact-sheet.pdf
12. Van der Noot, N., Ijspeert, A.J., Ronsse, R.: Bio-inspired controller achieving forward speed modulation with a 3D bipedal walker. Int. J. Robot. Res. **37**(1), 168–196 (2018)
13. Sreenath, K., Park, H.W., Poulakakis, I., Grizzle, J.W.: A compliant hybrid zero dynamics controller for stable, efficient and fast bipedal walking on MABEL. Int. J. Robot. Res. **30**(9), 1170–1193 (2011)
14. Rezazadeh, S., Hurst, J.W.: Control of ATRIAS in three dimensions: walking as a forced-oscillation problem. Int. J. Robot. Res. (2020). https://doi.org/10.1177/0278364920916777
15. Seok, S., Wang, A., Chuah, M.Y., Hyun, D.J., Lee, J., et al.: Design principles for energy-efficient legged locomotion and implementation on the MIT cheetah robot. IEEE/ASME Trans. Mechatron. **20**(3), 1117–1129 (2014)
16. Rohmer E., Singh S. P., and Freese M.: V-REP: A versatile and scalable robot simulation framework. in *IEEE/RSJ International Conference on Intelligent Robots and Systems (IROS)*, pp. 1321–1326, 2013.
17. Raibert, M.H.: Symmetry in running. Science **231**(4743), 1292–1294 (1986)
18. Wisse M., Atkeson C. G., and Kloimwieder D. K.: Swing leg retraction helps biped walking stability. in *IEEE-RAS International Conference on Humanoid Robots (Humanoids)*, pp. 295–300, 2005.